Submitted to *Inorg. Chem.* as an article

Effect of Heteroatoms on Field-Induced Slow Magnetic Relaxation of Mononuclear Fe-III (S=5/2) Ions within Polyoxometalates.

Takuo Minato,† Daniel Aravena,*,‡ Eliseo Ruiz,§ Kazuya Yamaguchi,†
Noritaka Mizuno,† and Kosuke Suzuki*,†

†Department of Applied Chemistry, School of Engineering, The University of Tokyo, 7-3-1 Hongo, Bunkyo-ku, Tokyo 113-8656, Japan

‡Departamento de Química de los Materiales, Facultad de Química y Biología, Universidad de Santiago de Chile, Casilla 40, Correo 33, Santiago, Chile

§Departament de Química Inorgànica i Orgànica and Institut de Química Teòrica i Computacional, Universitat de Barcelona, Diagonal 645, 08028 Barcelona, Spain

ABSTRACT

In this paper, synthesis and magnetic properties of mononuclear Fe^{III}-containing polyoxometalates (POMs) $TBA_7H_{10}[(A\text{-}\alpha\text{-}XW_9O_{34})_2Fe]$ (**II**x, X = Ge, Si; TBA = tetra-*n*-butylammonium) with heteroatoms are reported. In these POMs, Fe^{III} ion coordinates to two trivacant lacunary units $[A\text{-}\alpha\text{-}XW_9O_{34}]^{10-}$ (X = Ge, Si) and shows a highly distorted six-coordinate octahedral geometry. These POMs exhibit field-induced single-molecule magnet properties based on the single high-spin Fe^{III} magnetic center (S = 5/2). Combining experiment and *ab initio* calculations, we investigated the effect of heteroatoms of the lacunary units on the single-molecule magnet properties of these POMs. By changing the heteroatoms from Si (**II**$_{Si}$) to Ge (**II**$_{Ge}$), the coordination geometry around the Fe^{III} ion is mildly changed. Concretely, the axial Fe–O bond length of **II**$_{Ge}$ is shortened compared with that of **II**$_{Si}$, and consequently the distortion from the ideal octahedral coordination geometry of **II**$_{Ge}$ is larger than that of **II**$_{Si}$. The effective demagnetization barrier of **II**$_{Ge}$ (11.4 K) is slightly larger than that of **II**$_{Si}$ (9.2 K). Multireference *ab initio* calculations predict zero-field splitting parameters in good agreement with experiment. Although the differences in the coordination geometries and magnetic properties of **II**$_{Ge}$ and **II**$_{Si}$ are quite small, *ab initio* calculations indicate subtle changes in the magnetic anisotropy which are in line with the observed magnetic relaxation properties.

INTRODUCTION

Polyoxometalates (POMs) are a class of anionic metal oxide clusters that exhibit large structural diversity, and their properties can be controlled by selecting structures, constituent elements, and charges.[1] Various types of metal cations can be introduced into the structurally well-defined vacant sites of lacunary POMs, where precise structural design of metal oxo clusters is possible; *i.e.*, numbers, arrangements, and coordination geometries of metal cations can be designed within the vacant sites. Therefore, lacunary POMs are useful ligands for the rational investigation of catalytic, redox, and magnetic properties of metal oxo clusters.[2] In particular, since the coordination geometries of metal cations directly affect their electron configurations, rigid multidentate lacunary POM ligands are useful to design and control their magnetic properties.[3] We have recently reported that various mononuclear and multinuclear metal oxo clusters can be selectively synthesized using lacunary POMs in organic solvents.[4,5] In particular, a mononuclear Fe^{III} ion possessing an unusually distorted six-coordinate octahedral geometry within a trivacant lacunary POM exhibited a unique field-induced single-molecule magnet (SMM) property for a high spin Fe^{III} ion.[4] *Ab initio* calculations showed that the axial ligand elongations of the octahedrally coordinated $[FeO_6]^{9-}$ unit destabilized the $d_{x^2-y^2}$ orbital, which lowered the sextet–quartet gap, resulting in a large magnetic anisotropy of the Fe^{III} ion required

for SMMs.[6] It is noteworthy that although a number of reports of mononuclear SMMs consisted of 3d transition metals have been reported,[7] there have been only two reports on mononuclear Fe^{III} complexes exhibiting SMM properties[8] other than our mononuclear Fe^{III}-POM, to the best of our knowledge: *i.e.*, Mossin, Mindiola, and coworkers reported [(PNP)$FeCl_2$] (PNP = N[2-$P(CHMe_2)_2$-4-methylphenyl]$_{2-}$)[8a] and Nocera and coworkers reported $(PR_3)_2FeCl_3$ (R = Me or Me_2Ph).[8b] Both examples are associated with intermediate spin Fe^{III} (S = 3/2), in contrast with our compound that is based on high spin Fe^{III} (S = 5/2).

To date, several experimental and theoretical studies have revealed that heteroatoms of POMs play important roles in controlling the catalytic and redox properties because the anion charges and/or the coordination geometries of POMs depend on the heteroatoms.[9] In magnetic molecules, a few comparative studies on POM-based SMMs with different heteroatoms have been reported;[10] *e.g.*, {Mn_6} clusters in [B-α-XW_9O_{34}]$_{10-}$ (X = Si, Ge) and {Co_{16}} clusters in [A-α-XW_9O_{34}]$_{n-}$ (X = P, Si, Ge). However, theoretical studies about the effect of heteroatoms on the magnetic properties are lacking. Herein, we synthesized octahedrally coordinated mononuclear Fe^{III}-containing POMs with different heteroatoms, TBA_7H_{10}[(A-α-XW_9O_{34})$_2$Fe] (**II**x, X = Ge, Si; TBA = tetra-*n*-butylammonium). These POMs showed field-induced slow magnetic relaxation characteristic for SMMs. Experimental and theoretical investigations revealed that by changing the heteroatom from Si to Ge, the coordination geometries of Fe^{III} ions in **II**x and their electronic structures were slightly changed, engendering a small enhancement of the SMM properties.

EXPERIMENTAL SECTION

Materials. Acetone (Kanto Chemical), 1,2-dichloroethane (Kanto Chemical), diethyl ether (Kanto Chemical), and $Fe(acac)_3$ (Aldrich) were used as received. TBA_4[A-α-$GeW_9O_{28}(OCH_3)_6$] (**I**$_{Ge}$)[11] and TBA_7H_{10}[(A-α-SiW_9O_{34})Fe] (**II**$_{Si}$)[4] were synthesized according to reported procedures.

Instruments. IR spectra were measured on JASCO FT/IR-4100 using KBr disks. UV/vis spectra were measured on JASCO V-570. Cold-spray ionization (CSI) mass spectra were recorded on JEOL JMS-T100CS. Thermogravimetric and differential thermal analyses (TG-DTA) were performed on Rigaku Thermo plus TG 8120. ICP-AES analyses for Fe, Ge, and W were performed on Shimadzu ICPS-8100. Elemental analyses were performed on Elemental vario MICRO cube (for C, H, and N) at the Elemental Analysis Center of School of Science of the University of Tokyo.

X-ray Crystallography. Diffraction measurements were made on a Rigaku MicroMax-007 Saturn 724 CCD detector with graphic monochromated Mo Kα radiation (λ = 0.71069 Å, 50 kV, 24 mA) at 123 K. The data were collected and processed using CrystalClear[12] and HKL2000.[13] Neutral scattering factors were obtained from the standard source. In the reduction of data, Lorentz and polarization

corrections were made. The structural analyses were performed using CrystalStructure[14] and WinGX.[15] All structures were solved by SHELXS-97 (direct methods) and refined by SHELXL-2014.[16] The metal atoms (Fe, Ge, and W) and oxygen atoms in the POM frameworks were refined anisotropically. CCDC-1824491 (**II$_{Ge}$**) and CCDC-1035329 (**II$_{Si}$**) contains the supplementary crystallographic data for this paper. The data can be obtained free of charge via www.ccdc.cam.ac.uk/conts/retrieving.html (or from the Cambridge Crystallographic Data Centre, 12, Union Road, Cambridge CB2 1EZ, UK; Fax: (+44) 1223-336-033; or deposit@ccdc.cam.ac.uk).

Bond Valence Sum (BVS) Calculations. The BVS values were calculated by the expression for the variation of the length r_{ij} of a bond between two atoms i and j in observed crystal with valence V_i.

$$V_i = \sum_j \exp\left(\frac{r_0' - r_{ij}}{B}\right)$$

where B is constant equal to 0.37 Å, r'_0 is bond valence parameter for a given atom pair.[17]

Magnetic Susceptibilities. Magnetic susceptibilities of polycrystalline samples were measured on Quantum Design MPMS-XL7. Direct current (dc) magnetic susceptibility measurements were carried out between 1.9 and 300 K under 0.1 T magnetic field. Diamagnetic corrections were applied by the diamagnetisms of the sample holder and **I$_{Ge}$**. Alternating current (ac) magnetic susceptibility measurements were carried out under 0.1 T dc field and 3.96 × 10^{-4} T ac oscillating field. Variable-field (1–7 T) magnetization measurements were carried out in the temperature range of 1.9–10 K.

Synthesis of TBA$_7$H$_{10}$[(A-α-GeW$_9$O$_{34}$)$_2$Fe]·3H$_2$O (II$_{Ge}$). To Fe(acac)$_3$ (5.2 mg, 14.8 μmol) in mixture of acetone and water (24:1, v/v, 3 mL, **I$_{Ge}$** (100 mg, 29.5 μmol, 2.0 equiv. with respect to Fe(acac)$_3$) was added, and the resulting solution was stirred for 5 h at room temperature (ca. 20°C). Then, diethyl ether (50 mL) was added. Pale yellow precipitates formed were filtered off, followed by recrystallization from a mixture of 1,2-dichloroethane and diethyl ether. Pale yellow crystals of **II$_{Ge}$** suitable for X-ray crystallographic analysis were obtained (33.8 mg, 36% yield based on **I$_{Ge}$**). Positive-ion MS (CSI, 1,2-dichloroethane): *m/z* 3350 (calcd. 3350.2) [TBA$_9$Ge$_2$W$_{18}$O$_{63}$Fe]$^{2+}$, 6458 (calcd. 6457.9) [TBA$_8$Ge$_2$W$_{18}$O$_{63}$Fe]$^+$. IR (KBr pellet): 1635, 1380, 1152, 1107, 1061, 1014, 992, 954, 889, 814, 772, 737, 683, 561, 524, 360, 338, 321 cm^{-1}. Elemental analysis, calcd (%) for C$_{114}$H$_{270}$Cl$_2$FeGe$_2$N$_7$O$_{70}$W$_{18}$ (TBA$_7$H$_{10}$[(GeW$_9$O$_{34}$)$_2$Fe]·3H$_2$O): C, 21.15; H, 4.25; N, 1.54; Ge, 2.28; Fe, 0.88; W, 52.03. Found: C, 21.24; H, 4.23; N, 1.52; Ge, 2.29; Fe, 0.89; W, 53.05.

Computational Details. Electronic structure calculations were performed by means of the ORCA 4.0.1.2 program.[18] Complete active space self-consistent field (CASSCF)[19] calculations were converged for two different active spaces: (i) a (5,5) model including all 3d orbitals of the Fe^{III} center and (ii) a (9,7) model that also includes the five 3d orbitals but also considers the bonding combinations between the e$_g$ d orbitals and the adequate linear combinations of ligand orbitals

yielding an essentially σ-type metal-ligand interaction. N-electron valence state perturbation theory (NEVPT2)[20] correction to CASSCF energies was included to account for dynamic correlation. Scalar relativistic effects were described by the second order Douglas-Kroll-Hess Hamiltonian (DKH2).[21] Spin-orbit-coupling (SOC) mixing was considered by state interaction between converged CASSCF states (Quasi degenerate perturbation theory method). CASSCF(5,5) calculations included 1 sextet, 24 quartets and 75 doublets. CASSCF(9,7) calculations included 11 sextets and 24 quartets. To construct the model, atoms connected the Fe^{III} center by three bonds or less were kept their position determined by X-ray diffraction. Dangling bonds were completed with hydrogen atoms, which were optimized using the BP86 density functional.[22] Multireference calculations were carried out using the recontracted versions of the def2-TZVP all electron basis set available in ORCA. DFT optimizations were performed using the def2-TZVP basis set.[23] To speed up calculations, resolution of the identity (RI) approximation[24] was considered in conjunction with their corresponding auxiliary basis sets.[25] The splitting of d-orbitals for CASSCF(5,5) calculations was derived from *ab initio* ligand filed theory (AILFT).[26] This method employs the configuration interaction matrix to map each matrix element to the corresponding ligand field matrix. In this way, interelectronic repulsion and ligand field parameters can be obtained by least-squares minimization.

RESULTS AND DISCUSSION

Synthesis of Fe^{III}-Containing POMs. We have recently synthesized an organic-solvent soluble Ge-centered trivacant lacunary POM and isolated it as a methoxide form ($TBA_4[A\text{-}\alpha\text{-}GeW_9O_{28}(OCH_3)_6]$, $\mathbf{I_{Ge}}$).[11] As mentioned in our previous report, the methoxy groups of $TBA_4[A\text{-}\alpha\text{-}SiW_9O_{28}(OCH_3)_6]$ ($\mathbf{I_{Si}}$) were easily hydrolyzed in organic media even by the presence of trace amounts of water, showing that $\mathbf{I_{Si}}$ could be used as a precursor of metal substituted POMs. Based on these results, a mononuclear Fe^{III}-containing germanotungstate ($\mathbf{II_{Ge}}$) was synthesized by reacting $\mathbf{I_{Ge}}$ with 0.5 equivalents of $Fe(acac)_3$ in a mixture of acetone and water (96:4, v/v) (Figure 1). Single crystals of $\mathbf{II_{Ge}}$ suitable for X-ray crystallographic analysis were obtained from a mixture of 1,2-dichloroethane and diethyl ether. The crystallographic analysis revealed that the anion structure of $\mathbf{II_{Ge}}$ was a mononuclear Fe-containing S-shaped dimer possessing vacant sites and essentially isostructural with that of $TBA_7H_{10}[(A\text{-}\alpha\text{-}SiW_9O_{34})_2Fe]$ ($\mathbf{II_{Si}}$)[4] except for the heteroatom ($\mathbf{II_{Ge}}$, Ge; $\mathbf{II_{Si}}$, Si) (Figures 1, S1, Table 1). Seven TBA cations were observed in the crystallographic analysis in agreement with the results of the elemental analyses. The bond valence sum values of $\mathbf{II_{Ge}}$ for W (5.93–6.61), Ge (4.12), and Fe (2.83) indicate that the respective valences are +6, +4, and +3 (Table S1). These values are similar to those of $\mathbf{II_{Si}}$ for W (6.02–6.19), Si (3.97), and Fe (2.90).[4]

Table 1. Crystallographic data for **II$_{Ge}$** and **II$_{Si}$**

Compound	**II$_{Ge}$**	**II$_{Si}$**
formula	$C_{116}Cl_4FeGe_2N_7O_{72}W_{18}$	$C_{116}Cl_4FeN_7O_{72}Si_2W_{18}$
Fw (g mol^{-1})	6295.36	6206.36
crystal system	monoclinic	monoclinic
space group	*C*2/*c* (#15)	*C*2/*c* (#15)
a (Å)	35.7121(3)	35.5945(2)
b (Å)	14.5597(2)	14.48620(10)
c (Å)	38.5030(3)	38.2599(2)
α (deg)	90	90
β (deg)	114.0479(2)	113.9049(3)
γ (deg)	90	90
V (Å^3)	18282.3(3)	18035.63(19)
Z	4	4
temp (K)	123(2)	123(2)
ρ_{calcd} (g cm^{-3})	2.287	2.286
GOF	1.121	1.115
R_1 [$I>2\sigma(I)$]^a	0.0768	0.0424
wR_2 ^{a}	0.2221	0.0994

^{a} $R_1 = \Sigma||F_o|-|F_c||/\Sigma|F_o|$, $wR_2 = \{\Sigma\,[w(F_{o2}-F_{c2})]/\,\Sigma\,[w(F_{o2})_2]\}_{1/2}$.

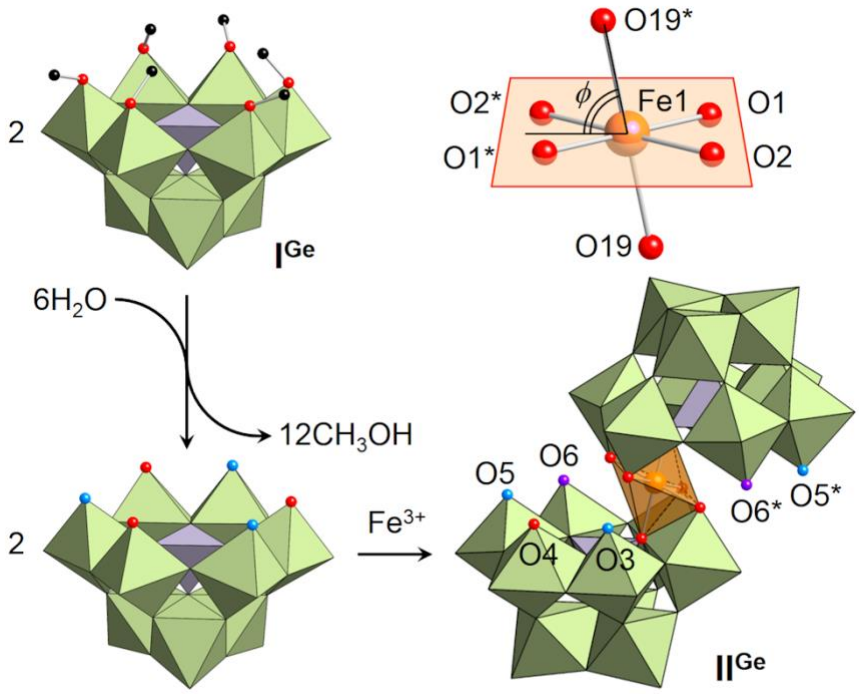

Figure 1. Schematic of the synthesis of **II**$_{Ge}$ by reacting **I**$_{Ge}$ with Fe(acac)$_3$. Light green, gray, and orange polyhedra represent $[WO_6]^{6-}$, $[GeO_4]^{4-}$, and $[FeO_6]^{3-}$, respectively. Red, purple, blue, black, and orange spheres represent O, OH, OH_2, C, and Fe, respectively.

The coordination geometry of the introduced Fe^{III} ion was six-coordinate distorted octahedral: *i.e.*, the Fe^{III} ion was coordinated by four equatorial oxygen atoms (O1, O1*, O2, O2*) and two axial oxygen atoms (O19, O19*). Notably, the coordination geometries of **II**$_{Ge}$ were slightly different from those of **II**$_{Si}$: By changing the heteroatom (X) from Si to Ge, the X–O bond lengths (**II**$_{Ge}$, 1.720–1.749 Å; **II**$_{Si}$, 1.610–1.645 Å) were elongated owing to the larger ionic radius of Ge^{IV} (Table 2), which was the same trend as those of **I**$_X$.[11] The axial Fe–O bond lengths (Fe1–O19; **II**$_{Ge}$, 2.058 Å; **II**$_{Si}$, 2.099 Å) were shortened while the equatorial Fe–O bond lengths (Fe1–O1, Fe1–O2; **II**$_{Ge}$, 2.020, 2.033 Å; **II**$_{Si}$, 1.991, 2.003 Å) were moderately elongated (Table 2). The distortion angles of the axial ligands against the equatorial planes (ϕ; **II**$_{Ge}$, 74.5°; **II**$_{Si}$, 75.8°) decreased slightly (Table 2), thus showing that the distortion of the Fe^{III} ion from the ideal six-coordinate octahedral geometry in **II**$_{Ge}$ was larger than that in **II**$_{Si}$. In the case of **II**$_{Ge}$, The intermolecular shortest Fe···Fe distance of **II**$_{Ge}$ was 14.560 Å (Figure S2a), and this value was similar to that of **II**$_{Si}$ (14.486 Å, Figure S2b), showing that each paramagnetic Fe^{III} ion was separated. The CSI mass spectrum of **II**$_{Ge}$ in acetonitrile showed signal sets centered at *m/z* 3350 and 6458 assignable to $[TBA_9Ge_2W_{18}O_{63}Fe]^{2+}$ and $[TBA_8Ge_2W_{18}O_{63}Fe]^{+}$, respectively (Figure S3), supporting that **II**$_{Ge}$ was selectively synthesized and stable in this solvent. The UV/vis absorption spectrum of **II**$_{Ge}$ in acetonitrile showed a broad band at 350 nm assignable to LMCT transition of the $[FeO_6]^{9-}$ unit. The LMCT absorption band was observed at slightly shorter

wavelength in the case of **II**$_{Si}$ (345 nm) (Figure S4). All the above mentioned results, the elemental analyses, and TG-DTA data showed that the formula of **II**$_{Ge}$ is $TBA_7H_{10}[(A\text{-}\alpha\text{-}GeW_9O_{34})_2Fe]\cdot 3H_2O$.

Table 2. Selected bond lengths (Å) and distortion angles (°) for **II**$_{Ge}$ and **II**$_{Si}$

	II$_{Ge}$	**II**$_{Si}$
Fe1–O1	2.033	2.003
Fe1–O2	2.020	1.991
Fe1–O19	2.058	2.099
X1–O19	1.745	1.638
X1–O20	1.737	1.617
X1–O21	1.720	1.610
X1–O22	1.749	1.645
distortion angle (ϕ)	74.5	75.8

Magnetic Properties of Mononuclear Fe^{III}-Containing POMs. DC magnetic susceptibility of the polycrystalline samples under 0.1 T showed that χT values of **II**$_{Ge}$ and **II**$_{Si}$ at 300 K were 4.15 and 4.35 cm^3 K mol^{-1}, respectively (Figure S5).[4] These values are close to the spin-only value for a high-spin Fe^{III} ion (4.37 cm^3 K mol^{-1}; S = 5/2, g = 2.00), supporting the valence of Fe^{III}. The M vs. HT^{-1} data showed the presence of magnetic anisotropy in **II**$_{Ge}$ and **II**$_{Si}$ (Figure 3). The M vs. HT^{-1} data was fitted by using the PHI program[27] adopting the anisotropic Hamiltonian (H) given by the following equation with the parameters of the axial (D) and transverse (E) magnetic anisotropies and Landé g-factor:

$$H = D\{S_z^2 - S(S + 1)/3\} + E(S_x^2 - S_y^2) + \mu_B g\mathbf{SH}$$

The best fitting parameters for **II**$_{Ge}$ and **II**$_{Si}$ were obtained as follows: D = –1.26 cm^{-1}, E = –4.76 × 10^{-1} cm^{-1}, $g_x = g_y$ = 1.58, g_z = 2.53 for **II**$_{Ge}$ (Figure 3a) and D = –1.22 cm^{-1}, E = –2.48 × 10^{-1} cm^{-1}, $g_x = g_y$ = 1.80, g_z = 2.05 for **II**$_{Si}$ (Figure 3b). The axial magnetic anisotropy parameter $|D|$ of **II**$_{Ge}$ was slightly larger than that of **II**$_{Si}$, indicating that the change of coordination geometries of Fe^{III} ions affects the magnetic properties. From a phenomenological point of view, these parameters accurately reproduce magnetization data. However, the large anisotropy of the g-values appears unlikely for an Fe^{III} ion. We attempted to fit the magnetization curves using an isotropic g-values and found a reasonable match with experiment, although not as accurate as the former fit due to the lower number of fitting variables.

The ac magnetic susceptibility of **II**$_{Ge}$ under the external dc magnetic field of 0.1 T showed temperature- and frequency-dependence of χ' and χ'', indicating the field-induced slow relaxation of magnetization characteristic for SMMs (Figures 2a and S6). The Cole−Cole plots for **II**$_{Ge}$ in the form of χ'' versus χ' were fitted by means of the generalized Debye model,[28] which showed the small α values in the range of 0.06−0.09, thus indicating a single relaxation process (Figure S7). According to the Arrhenius plot, the energy barrier for the magnetization reversal of **II**$_{Ge}$ was 11.4 K ($\tau_0 = 1.3 \times 10^{-6}$ s). This value was slightly higher than that of **II**$_{Si}$ (9.2 K, $\tau_0 = 3.3 \times 10^{-6}$ s) presumably owing to the larger *D* value of **II**$_{Ge}$ (Figure 2b).[4]

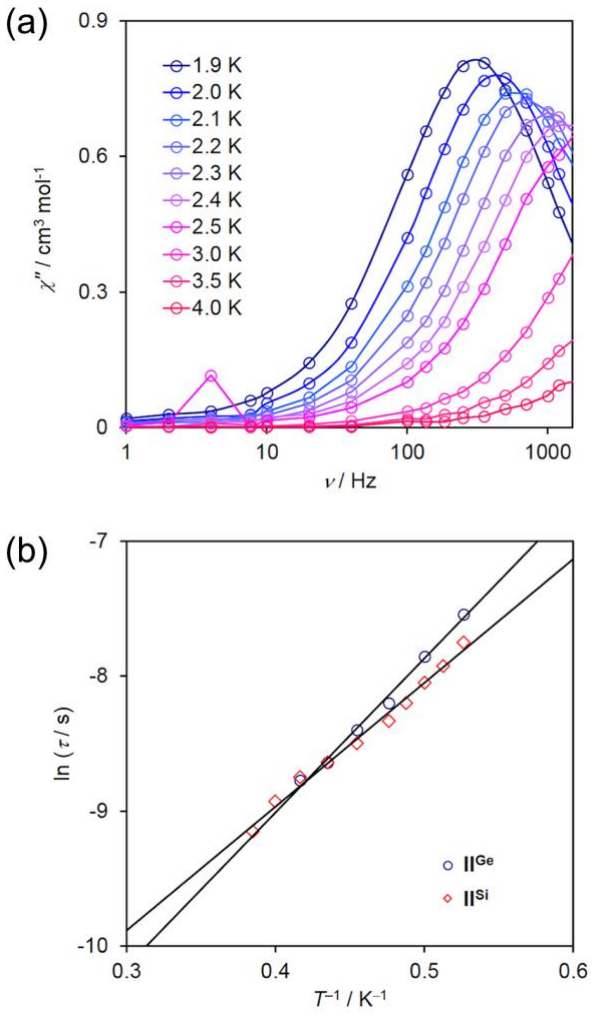

Figure 2. (a) Frequency dependences of χ'' for **II**$_{Ge}$ under 0.1 T external dc field. (b) Plots of relaxation time (τ) versus T^{-1} for **II**$_{Ge}$. The solid lines represent the best fit with the Arrhenius law ($\ln\tau$ ($\tau = \tau_0 \exp(U_{eff}/k_B T)$) vs. T^{-1}) at the thermally activated regime.

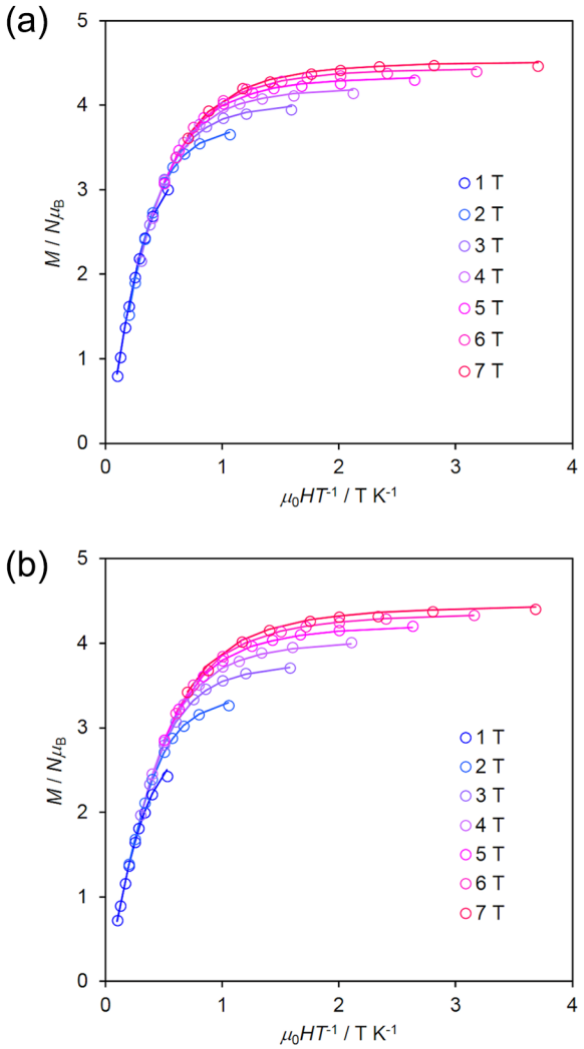

Figure 3. Low temperature magnetization data for (a) **II**$_{Ge}$ and (b) **II**$_{Si}$. Solid lines represent the best fits obtained by PHI program.

***Ab initio* calculations.** Next, to investigate the electronic structures of **II**$_{Ge}$ and **II**$_{Si}$, multireference *ab initio* calculations were carried out. Since the size of the lacunary POM ligands prevented the calculation of the full complexes, model structures were constructed for both molecules (Figure 4a), where atomic positions were obtained from the corresponding crystallographic structures (Figure S1).[4] The Fe^{III} ions and all atoms at a distance equal or under three covalent bonds from the Fe^{III} ions were retained in the model structure. Dangling bonds for atoms at the frontier of the model were completed with hydrogens, which positions were optimized. CASSCF(5,5) and CASSCF(9,7) calculations were performed for **II**$_{Ge}$ and **II**$_{Si}$, where the smaller active space corresponds to the five 3d orbitals of the Fe^{III} ions and the extended model incorporates the bonding counterparts of the d_{x2-y2} and d_{z2} orbitals. Dynamical correlation was taken into account by the NEVPT2 method and spin-orbit effects were considered by a quasi-degenerate perturbation theory (QDPT) step for state interaction due to the electronic spin-orbit coupling operator (see Computational Details section for further

information). *Ab initio* ligand field theory analysis pictures a qualitatively similar d-orbital splitting for **II**$_{Ge}$ and **II**$_{Si}$ (Figure 4b). From the CASSCF(5,5) energies and wave functions, AILFT yields d-orbital energies which are more consistent with a square planar coordination than with an octahedral geometry. This is in line with the axially elongated Fe–O distance associated to the more exposed position of equatorial oxygen donor atoms in comparison to the axial oxygen atoms (Table 2).[29] Given the more pronounced axial elongation of **II**$_{Si}$, the total orbital energy splitting for this complex is larger than **II**$_{Ge}$. In both cases, d_{xy} and d_{yz} orbitals are lower in energy and almost degenerate, with an energy separation of 397.7 cm^{-1} (**II**$_{Ge}$) and 239.3 cm^{-1} (**II**$_{Si}$). The third orbital is mainly d_{xy}, with an energy of 4316.9 cm^{-1} (**II**$_{Ge}$) and 4382.8 cm^{-1} (**II**$_{Si}$). The d_{z^2} orbitals are the most differing, as they appear at 9211.9 cm^{-1} (**II**$_{Ge}$) and 7962.3 cm^{-1} (**II**$_{Si}$). Finally, the antibonding $d_{x^2-y^2}$ orbitals are at 17733.9 cm^{-1} (**II**$_{Ge}$) and 18771.3 cm^{-1} (**II**$_{Si}$) (Figure 4b). As noted in our previous theoretical investigations,[6] zero-field splitting parameters of high spin d^5 complexes tend to be underestimated by CASSCF calculations as they chiefly depend on the sextet-quartet energy gap, which is overestimated under this methodology. As expected, NEVPT2 calculations tend to improve results, although their correction is only partial.

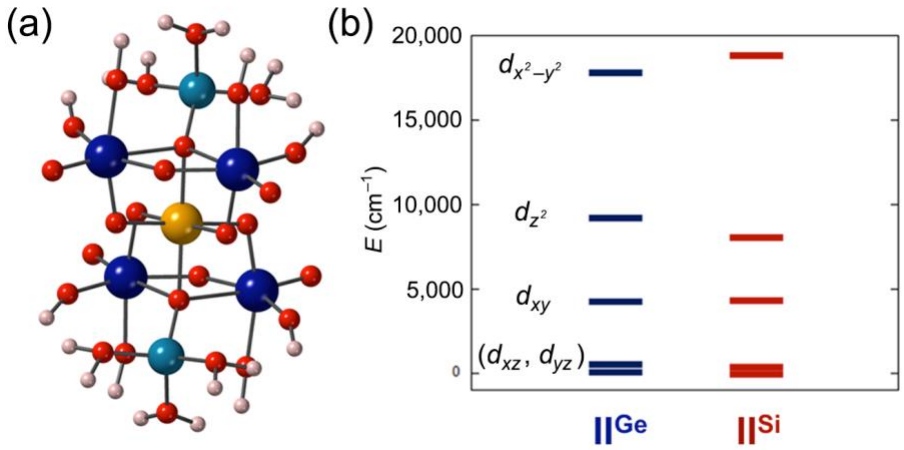

Figure 4. (a) Calculated model structure of **II**$_{Ge}$, the model for **II**$_{Si}$ is analogous. Color code: W: dark blue, Fe: orange, Ge: blue, O: red, H: pink. (b) AILFT d-orbital splitting obtained from NEVPT2 energies on top of a CASSCF(5,5) calculation.

To account for these limitations, CASSCF(9,7) calculations were performed including the bonding complement of the antibonding $d_{x^2-y^2}$ and d_{z^2} orbitals. 11 sextet and 24 quartet roots where included in the state average orbital optimization. In this way, 10 of the sextet roots are LMCT states, which will give a higher weight of charge transfer configurations and lower the sextet-quartet gap. Of course, the inclusion of more LMCT roots will increasingly bias the result in this direction, potentially leading to calculation artifacts. To prevent from this possibility, LMCT transitions were calculated, which are in

reasonable agreement with experimental UV/vis spectra (Figure S4, Table S2). Considering NEVPT2 energies, the sextet-quartet gaps are 8784 cm^{-1} and 8478 cm^{-1}, while the zero-field splitting parameters (D) are –1.07 cm^{-1} and –1.01 cm^{-1} for **II$_{Ge}$** and **II$_{Si}$**, respectively (Table S3). These values are in close agreement with the experimental fit for **II$_{Ge}$** (–1.26 cm^{-1}) and **II$_{Si}$** (–1.22 cm^{-1}). Then, axial magnetic anisotropy is slightly smaller for **II$_{Si}$** in comparison to **II$_{Ge}$**. In addition, calculations indicate that E/D is lower for **II$_{Ge}$** (0.056) in comparison to **II$_{Si}$** (0.083), in line with the observed enhancement of SMM properties for **II$_{Ge}$** (Figure 2b). Although the differences in spin Hamiltonian parameters are small for both complexes, the trend of a higher axiality for **II$_{Ge}$** shows up independently of the active space (5,5 or 9,7) for both CASSCF and NEVPT2 energies.

The orientation of the anisotropy axis matches the vector connecting the axial donor atoms (Figure 5). The alignment with the z-axis can be rationalized if we consider the sextet-quartet excitations which are responsible for magnetic anisotropy in a high spin d^5 ion. In the free ion limit, the ground ^6S term mixes with the ^4P excited term by the SOC operator. Under a square planar ligand field, the ^4P term will split in $^4A_2$ and ^4E states and mix with levels stemming from the other quartet terms. Spin-orbit coupling mixing to the $^4A_2$ level will be related with l_z and ^4E state interaction will be related to $l_{x,y}$ (see Figure 6). Thus, the difference in the x and y directions due to the structural distortion will be related with the presence of a nonzero component for the rhombic zero-field splitting parameter (E). This rhombic contribution favors the quantum tunneling contribution resulting in a faster magnetic relaxation worsening SMM properties. In the case of **II$_{Si}$** and **II$_{Ge}$**, several excitations contribute to D and E, given their departure from square planar geometry. As expected, sextet-quartet excitations contribute more than sextet-sextet transitions to zero-field splitting parameters, especially for E (Tables S3). Table S4 shows the contribution of all quartet and sextet states to D and E for **II$_{Si}$** and **II$_{Ge}$**. Although the final D and E parameters results for the sum (or cancellation) of many contributions, it is possible to appreciate how cancellation of contributions to E is less effective in **II$_{Si}$** when comparing with **II$_{Ge}$**. Finally, we stress that the relatively good agreement between the calculated magnetic anisotropy properties with the experimental data does not guarantee a quantitative prediction due to the small energy differences involves for these systems.

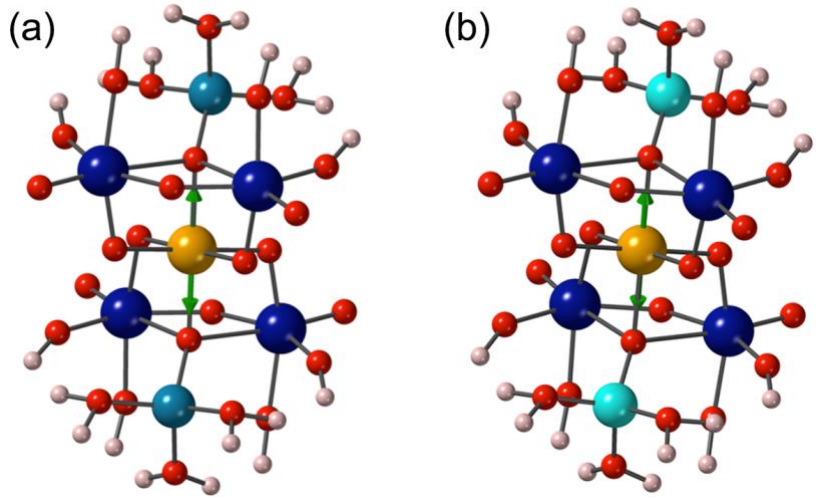

Figure 5. Orientation of the z-axis of the zero-field splitting tensor of $\mathbf{II_{Ge}}$ and $\mathbf{II_{Si}}$. Color code: W: dark blue, Fe: orange, Ge: blue, Si: light blue, O: red, H: pink. Values are based on NEVPT2 energies on top of a CASSCF(9,7) calculation. *D* tensor was obtained by the second order perturbation theory approach.

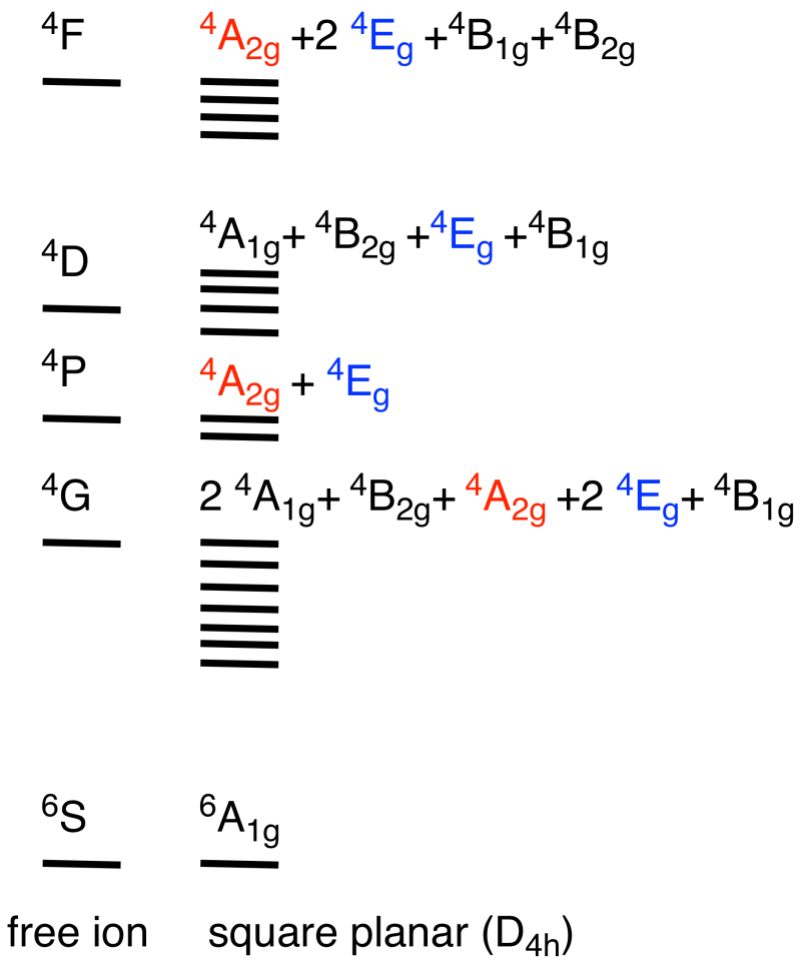

Figure 6. Free ion terms and their splitting under D_{4h} symmetry for a high-spin d^5 configuration. The excited states involved in SOC contribution are highlighted in color, blue for the E_g states (through the l_x and l_y operators) and red for the A_{2g} states (l_z operator).

CONCLUSION

We synthesized Fe^{III}-containing POMs $TBA_7H_{10}[(A\text{-}\alpha\text{-}XW_9O_{34})Fe]$ (**II**$_X$, X = Ge, Si) and investigated the effect of heteroatoms on their magnetic properties. These POMs possessed mononuclear Fe^{III} ions with distorted six-coordinate octahedral coordination geometries and showed field-induced SMM properties. By changing the heteroatoms from Si to Ge in **II**$_X$, the coordination geometries of Fe^{III} ions were mildly changed; the axial Fe–O bond length of **II**$_{Ge}$ was shortened compared with that of **II**$_{Si}$ and the distortion from the ideal octahedral coordination geometry of **II**$_{Ge}$ was larger than that of **II**$_{Si}$. Changes in the coordination geometries engendered the slightly larger magnetic anisotropy for **II**$_{Ge}$, likely resulting in the increase in the energy barrier of the magnetization reversal. Although the difference in coordination geometries and the magnetic properties of **II**$_{Ge}$ and **II**$_{Si}$ were small, the small changes of magnetic properties were consistent with that of the theoretical results. Multireference calculations provide similar values of the zero-field splitting parameters for both compounds, with **II**$_{Ge}$ presenting moderately larger and more axial parameters. *E*/*D* ratio shows to be sensitive to the deviation of the coordination environment from the ideal elongated octahedral geometry.

ASSOCIATED CONTENT

Supporting Information

The Supporting Information is available free of charge on the ACS Publications website.

Crystallographic data, CSI mass spectrum, UV/vis spectra, magnetic data, and cartesian coordinates of molecular models for electronic structure calculations (PDF)

AUTHOR INFORMATION

Corresponding Authors

*E-mail: daniel.aravena.p@usach.cl

*E-mail: ksuzuki@appchem.t.u-tokyo.ac.jp

Notes

The authors declare no competing financial interest.

ACKNOWLEDGMENTS

This work was supported in part by JSPS KAKENHI Grant Numbers 17H03037, 15J09840. T. M. was supported by the JSPS through a Research Fellowship for Young Scientists. D.A. thanks FONDECYT Regular 1170524 project for financial support. Powered@NLHPC: This research was partially supported by the supercomputing infrastructure of the NLHPC (ECM-02) (Leftraru and UsachHPC servers). E.R. thanks Spanish *Ministerio de Economía y Competitividad* (grant CTQ2015-64579-C3-1-P, MINECO/FEDER, UE), Generalitat de Catalunya for 2017SGR1289 an ICREA Academia award and the computer resources in the Consorci Serveis Universitaris de Catalunya (CSUC).

REFERENCES

(1) (a) Thematic issue on polyoxometalates: Hill, C. L. *Chem. Rev.* **1998**, *98*, 1. (b) Miras, H. N.; Yan, J.; Long, D.-L.; Cronin, L. Engineering polyoxometalates with emergent properties. *Chem. Soc. Rev.* **2012**, *41*, 7403. (c) van Eldik, R.; Cronin, L. Eds. *Advances in Inorganic Chemistry*, Elsevier Academic Press, Amsterdam, 2017, vol. 69.

(2) (a) Zheng, S.-T.; Yang, G.-Y. Recent advances in paramagnetic-TM-substituted polyoxometalates (TM = Mn, Fe, Co, Ni, Cu). *Chem. Soc. Rev*. **2012**, *41*, 7623. (b) Bassil, B. S.; Kortz, U. Recent Advances in Lanthanide-Containing Polyoxotungstates. *Z. Anorg. Allg. Chem.* **2010**, *636*, 2222. (c) Ritchie, C.; Boskovic, C. *Polyoxometalates as Ligands for Functional Lanthanoid Complexes*, in *Polyoxometalate Chemistry: Some Recent Trends*; Sécheresse, F. Ed.; World Scientific, Singapore, 2013, 201. (d) Mizuno, N.; Yamaguchi, K.; Kamata, K. Epoxidation of olefins with hydrogen peroxide catalyzed by polyoxometalates. *Coord. Chem. Rev.* **2005**, *249*, 1944. (e) Sadakane, M.; Steckhan, E. Electrochemical Properties of Polyoxometalates as Electrocatalysts. *Chem. Rev*. **1998**, *98*, 219. (f) Clemente-Juan, J. M.; Coronado, E.; Gaita-Ariño, A. Magnetic polyoxometalates: from molecular magnetism to molecular spintronics and quantum computing. *Chem. Soc. Rev.* **2012**, *41*, 7464. (g) Kortz, U.; Müller, A.; Slageren, J. van; Schnack, J.; Dalal, N. S.; Dressel, M. Polyoxometalates: Fascinating structures, unique magnetic properties. *Coord. Chem. Rev.* **2009**, *253*, 2315.

(3) (a) Cardona-Serra, S.; Clemente-Juan, J. M.; Coronado, E.; Gaita-Ariño, A.; Camón, A.; Evangelisti, M.; Luis, F.; Martínez-Pérez, M. J.; Sesé, J. Lanthanoid Single-Ion Magnets Based on Polyoxometalates with a 5-fold Symmetry: The Series $[LnP_5W_{30}O_{110}]^{12-}$ (Ln^{3+} = Tb, Dy, Ho, Er, Tm, and Yb). *J. Am. Chem. Soc.* **2012**, *134*, 14982. (b) AlDamen, M. A.; Clemente-Juan, J. M.; Coronado, E.; Martí-Gastaldo, C.; Gaita-Ariño, A. Mononuclear Lanthanide Single-Molecule Magnets Based on Polyoxometalates. *J. Am. Chem. Soc.* **2008**, *130*, 8874.

(4) Sato, R.; Suzuki, K.; Minato, T.; Shinoe, M.; Yamaguchi, K.; Mizuno, N. Field-induced slow magnetic relaxation of octahedrally coordinated mononuclear Fe(III)-, Co(II)-, and Mn(III)-containing polyoxometalates. *Chem. Commun.* **2015**, *51*, 4081.

(5) (a) Suzuki, K.; Sato, R.; Muzuno, N. Reversible switching of single-molecule magnet behaviors by transformation of dinuclear dysprosium cores in polyoxometalates. *Chem. Sci.* **2013**, *4*, 596. (b) Suzuki, K.; Tang, F.; Kikukawa, Y.; Yamaguchi, K.; Mizuno, N. Visible-Light-Induced Photoredox Catalysis with a Tetracerium-Containing Silicotungstate. *Angew. Chem., Int. Ed.* **2014**, *53*, 5356. (c) Suzuki, K.; Sato, R.; Minato, T.; Shinoe, M.; Yamaguchi, K.; Mizuno, N. A cascade approach to hetero-pentanuclear manganese-oxide clusters in polyoxometalates and their single-molecule magnet properties. *Dalton Trans.* **2015**, *44*, 14220. (d) Minato, T.; Suzuki, K.; Ohata, Y.; Yamaguchi, K.; Mizuno, N. A modular synthesis approach to multinuclear heterometallic oxo clusters in polyoxometalates. *Chem. Commun.* **2017**, *53*, 7533. (e) Minato, T.; Suzuki, K.; Yamaguchi, K.; Mizuno, N. Synthesis and Disassembly/Reassembly of Giant Ring-Shaped Polyoxotungstate Oligomers. *Angew. Chem., Int. Ed.* **2016**, *55*, 9630.

(6) Aravena, D.; Venegas-Yazigi, D.; Ruiz, E. Single-Molecule Magnet Properties of Transition-Metal Ions Encapsulated in Lacunary Polyoxometalates: A Theoretical Study. *Inorg. Chem.* **2016**, *55*, 6405. (b) Stavretis, S. E.; Atanasov, M.; Podlesnyak, A. A.; Hunter, S. C.; Neese, F.; Xue, Z.-L. Magnetic Transitions in Iron Porphyrin Halides by Inelastic Neutron Scattering and Ab Initio Studies of Zero-Field Splittings. *Inorg. Chem.* **2015**, *54*, 9790.

(7) For reviews, see: (a) Craig, G. A.; Murrie, M. 3d single-ion magnets. *Chem. Soc. Rev.* **2015**, *44*, 2135. (b) Frost, J. M.; Harriman, K. L. M.; Murugesu, M. The rise of 3-d single-ion magnets in molecular magnetism: towards materials from molecules? *Chem. Sci.* **2016**, *7*, 2470. (c) Gómez-Coca, S.; Aravena, D.; Morales, R.; Ruiz, E. Large magnetic anisotropy in mononuclear metal complexes. *Coord. Chem. Rev*. **2015**, *289*, 379.

(8) (a) Mossin, S.; Tran, B. L.; Adhikari, D.; Pink, M.; Heinemann, F. W.; Sutter, J.; Szilagyi, R. K.; Meyer, K.; Mindiola, D. J. A Mononuclear Fe(III) Single Molecule Magnet with a 3/2↔5/2 Spin Crossover. *J. Am. Chem. Soc.* **2012**, *134*, 13651. (b) Feng, X.; Hwang, S. J.; Liu, J.-L.; Chen, Y.-C.; Tong, M.-L.; Nocera, D. G. Slow Magnetic Relaxation in Intermediate Spin S = 3/2 Mononuclear Fe(III) Complexes. *J. Am. Chem. Soc.* **2017**, *139*, 16474.

(9) (a) Altenau, J. J.; Pope, M. T.; Prados, R. A.; So, H. Models for heteropoly blues. Degrees of valence trapping in vanadium(IV)- and molybdenum(V)-substituted Keggin anions. *Inorg. Chem.* **1975**, *14*, 417. (b) Pope, M. T.; Varga, G. M., Jr. Heteropoly Blues. I. Reduction Stoichiometries and Reduction Potentials of Some 12-Tungstates. *Inorg. Chem.* **1966**, *5*, 1249. (c) Maeda, K.; Katano, H.; Osakai, T.; Himeno, S.; Saito, A. Charge dependence of one-electron redox potentials of Keggin-type

heteropolyoxometalate anions. *J. Electroanal. Chem.* **1995**, *389*, 167. (d) Poblet, J. M.; López, X.; Bo, C.

Ab initio and DFT modelling of complex materials: towards the understanding of electronic and magnetic properties of polyoxometalates. *Chem. Soc. Rev.* **2003**, *32*, 297. (e) Maestre, J. M.; Lopez, X.; Bo, C.; Poblet, J.-M.; Casañ-Pastor, N. Electronic and Magnetic Properties of α-Keggin Anions: A DFT Study of $[XM_{12}O_{40}]^{n-}$, (M = W, Mo; X = Al^{III}, Si^{IV}, P^{V}, Fe^{III}, Co^{II}, Co^{III}) and $[SiM_{11}VO_{40}]^{m-}$ (M = Mo and W). *J. Am. Chem. Soc.* **2001**, *123*, 3749. (f) Mbomekallé, I.-M.; López, X.; Poblet, J. M.; Sécheresse, F.; Keita, B.; Nadjo, L. Influence of the Heteroatom Size on the Redox Potentials of Selected Polyoxoanions. *Inorg. Chem.* **2010**, *49*, 7001. (g) Quiñonero, D.; Wang, Y.; Morokuma, K.; Khavrutskii, L. A.; Botar, B.; Geletii, Y. V.; Hill, C. L.; Musaev, D. G. The Role of the Central Atom in Structure and Reactivity of Polyoxometalates with Adjacent d-Electron Metal Sites. Computational and Experimental Studies of γ -[(Xn+O4)RuIII2(OH)2(MFM)10O32](8-n)- for MFM = Mo and W, and X = AlIII, SiIV, PV, and SVI. *J. Phys. Chem. B* **2006**, *110*, 170. (h) Hu, C.; Hashimoto, M.; Okuhara, T.; Misono, M. Catalysis by Heteropoly Compounds .XXII. Reactions of Esters and Esterification Catalyzed by Heteropolyacids in a Homogeneous Liquid-Phase Effects of the Central Atom of Heteropolyanions Having Tungsten as the Addenda Atom. *J. Catal.* **1993**, *143*, 437. (i) Uehara, K.; Miyachi, T.; Nakajima, T.; Mizuno, N. Effects of Heteroatoms on Electronic States of Divanadium-Substituted γ-Keggin-type Polyoxometalates. *Inorg. Chem.* **2014**, *53*, 3907. (j) Uehara, K.; Taketsugu, T.; Yonehara, K.; Mizuno, N. Effects of Isolobal Heteroatoms in Divanadium-Substituted γ-Keggin-type Polyoxometalates on $(OV)_2(\mu\text{-}OH)_2$ Diamond and $(OV)_2(\mu\text{-}O)$ Core Structures and the Transformation. *Inorg. Chem.* **2013**, *52*, 1133. (k) Minato, T.; Suzuki, K.; Kamata, K.; Mizuno, N. Synthesis of α-Dawson-Type Silicotungstate [α-$Si_2W_{18}O_{62}]^{8-}$ and Protonation and Deprotonation Inside the Aperture through Intramolecular Hydrogen Bonds. *Chem. Eur. J.* **2014**, *20*, 5946. (l) Vilá-Nadal, L.; Mitchell, S. G.; Long, D.-L.; Rodríguez-Fortea, A.; López, X.; Poblet, J. M.; Cronin, L. Exploring the rotational isomerism in non-classical Wells–Dawson anions $\{W_{18}X\}$: a combined theoretical and mass spectrometry study. *Dalton Trans.* **2012**, *41*, 2264. (m) Vilá-Nadal, L.; Peuntinger, K.; Busche, C.; Yan. J.; Lüders, D.; Long, D.-L.; Poblet, J. M.; Guldi, D. M.; Cronin, L. Polyoxometalate $\{W_{18}O_{56}XO_6\}$ Clusters with Embedded Redox-Active Main-Group Templates as Localized Inner-Cluster Radicals. *Angew. Chem., Int. Ed.* **2013**, *52*, 9695.

(10) (a) Ritchie, C.; Ferguson, A.; Nojiri, H.; Miras, H. N.; Song, Y.-F.; Long, D.-L.; Burkholder, E.; Murrie, M.; Kögerler, P.; Brechin, E. K.; Cronin, L. *Angew. Chem., Int. Ed.* **2008**, *47*, 5609. (b) Ibrahim, M.; Lan, Y.; Bassil, B. S.; Xiang, Y.; Suchopar, A.; Powell, A. K.; Kortz, U. Hexadecacobalt(II)-Containing Polyoxometalate-Based Single-Molecule Magnet. *Angew. Chem., Int. Ed.* **2011**, *50*, 4708. (c) Ibrahim, M.; Haider, A.; Lan, Y.; Bassil, B. S.; Carey, A. M.; Liu, R.; Zhang,

G.; Keita, B.; Li, W.; Kostakis, G. E.; Powell, A. K.; Kortz, U. Multinuclear Cobalt(II)-Containing Heteropolytungstates: Structure, Magnetism, and Electrochemistry. *Inorg. Chem.* **2014**, *53*, 5179.

(11) Minato, T.; Suzuki, K.; Yamaguchi, K.; Mizuno, N. Alkoxides of Trivacant Lacunary Polyoxometalates. *Chem. Eur. J.* **2017**, *23*, 14213.

(12) (a) *CrystalClear* 1.3.6, Rigaku and Rigaku/MSC, The Woodlands, TX. (b) Pflugrath, J. W. The finer things in X-ray diffraction data collection. *Acta Crystallogr.* **1999**, *D55*, 1718.

(13) Otwinowski, Z.; Minor, W. Processing of X-ray Diffraction Data Collected in Oscillation Mode in *Methods in Enzymology*, C. W. Carter, Jr., R. M. Sweet, Eds., Macromolecular Crystallography, Part A, Academic press, New York, **1997**, *276*, 307.

(14) *CrystalStructure* 3.8, Rigaku and Rigaku/MSC, TheWoodlands, TX.

(15) Farrugia, L. J. WinGX suite for small-molecule single-crystal crystallography. *J. Appl. Crystallogr.* **1999**, *32*, 837.

(16) (a) Sheldrick, G. M. SHELX97, *Programs for Crystal Structure Analysis*, Release 97-2, University of Göttingen, Göttingen, Germany, **1997**. (b) Sheldrick, G. M. SHELX-2014, *Programs for Crystal Structure Analysis*, University of Göttingen, Göttingen, Germany, **2014**.

(17) (a) Brown, I. D.; Altermatt, D. Bond-valence parameters obtained from a systematic analysis of the Inorganic Crystal Structure Database. *Acta Crystallogr.* **1985**, *B41*, 244. (b) Brese, N. E.; O'Keeffe, M. Bond-valence parameters for solids. *Acta Crystallogr.* **1991**, *B47*, 192.

(18) Neese, F. Software update: the ORCA program system, version 4.0. *Wiley Interdiscip. Rev. Comput. Mol. Sci.* **2017**, *8*, e1327.

(19) Malmqvist, P.-Å.; Roos, B. O. The CASSCF state interaction method. *Chem. Phys. Lett.* **1989**, *155*, 189.

(20) (a) Angeli, C.; Cimiraglia, R.; Evangelisti, S.; Leininger, T.; Malrieu, J.-P. Introduction of n-electron valence states for multireference perturbation theory. *J. Chem. Phys.* **2001**, *114*, 10252. (b) Angeli, C.; Cimiraglia, R.; Malrieu, J.-P. N-electron valence state perturbation theory: a fast implementation of the strongly contracted variant. *Chem. Phys. Lett.* **2001**, *350*, 297.

(21) (a) Rösch, N.; Matveev, A.; Nasluzov, V. A.; Neyman, K. M.; Moskaleva, L.; Krüger, S. In Relativistic Electronic Structure Theory Part 2. Applications; Schwerdtfeger, P., Ed.; Elsevier, 2004; Vol. 14, pp 656−722. (b) Nakajima, T.; Hirao, K. The Douglas–Kroll–Hess Approach. *Chem. Rev.*

2012, *112*, 385. (c) Reiher, M. Relativistic Douglas–Kroll–Hess theory. *Wiley Interdiscip. Rev. Comput. Mol. Sci.* **2012**, *2*, 139.

(22) (a) Perdew, J. P. Density-functional approximation for the correlation energy of the inhomogeneous electron gas. *Phys. Rev. B:* **1986**, *33*, 8822. (b) Perdew, J. P. Erratum: Density-functional approximation for the correlation energy of the inhomogeneous electron gas. *Phys. Rev. B:* **1986**, *34*, 7406. (c) Becke, A. D. Density-functional exchange-energy approximation with correct asymptotic behavior. *Phys. Rev. A:* **1988**, *38*, 3098.

(23) Weigend, F.; Ahlrichs, R. Balanced basis sets of split valence, triple zeta valence and quadruple zeta valence quality for H to Rn: Design and assessment of accuracy. *Phys. Chem. Chem. Phys.* **2005**, *7*, 3297.

(24) (a) Whitten, J. L. Coulombic potential energy integrals and approximations. *J. Chem. Phys.* **1973**, *58*, 4496. (b) Dunlap, B. I.; Connolly, J. W. D.; Sabin, J. R. On first-row diatomic molecules and local density models. *J. Chem. Phys.* **1979**, *71*, 4993. (c) Neese, F. An improvement of the resolution of the identity approximation for the formation of the Coulomb matrix. *J. Comput. Chem.* **2003**, *24*, 1740.

(25) (a) Weigend, F. Accurate Coulomb-fitting basis sets for H to Rn. *Phys. Chem. Chem. Phys.* **2006**, *8*, 1057. (b) Pantazis, D. A.; Chen, X. Y.; Landis, C. R.; Neese, F. All-Electron Scalar Relativistic Basis Sets for Third-Row Transition Metal Atoms. *J. Chem. Theory Comput.* **2008**, *4*, 908.

(26) Atanasov, M.; Ganyushin, D.; Sivalingam, K.; Neese, F.; Atanasov, M.; Ganyushin, D.; Sivalingam, K.; Neese, F. In Molecular Electronic Structures of Transition Metal Complexes II; Mingos, D. M. P.; Day, P.; Dahl, J. P. Eds.; Structure and Bonding; Springer: Berlin/Heidelberg, Germany, 2012; ISBN 978-3-642-27377-3.

(27) Chilton, N. F.; Anderson, R. P.; Turner, L. D.; Soncini, A.; Murray, K PHI: A powerful new program for the analysis of anisotropic monomeric and exchange-coupled polynuclear d- and f-block complexes. S. *J. Comput. Chem.* **2013**, *34*, 1164.

(28) Gatteschi, D.; Sessoli, R.; Villain, J. *Molecular Nanomagnets*; Oxford University Press: Oxford, U.K., 2006.

(29) The structural model is not exactly the same with the previous one, however, the orbital pattern is essentially the same.

TABLE OF CONTENTS

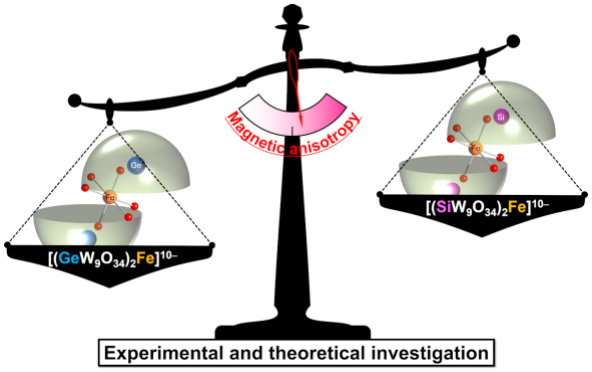

The effect of heteroatoms on single-molecule magnet properties of mononuclear high-spin Fe^{III} magnetic center within lacunary polyoxometalates was investigated by combining experiment and multireference *ab initio* calculations. By changing the heteroatoms from Si to Ge, the coordination geometry around the Fe^{III} ion is mildly changed, which engendered the slightly larger magnetic anisotropy, likely resulting in a small enhancement of the single-molecule magnet properties.